MAUSAM, **76**, 2 (April 2025), 577-590

MAUSAM

DOI : https://doi.org/10.54302/mausam.v76i2.6596
Homepage: https://mausamjournal.imd.gov.in/index.php/MAUSAM

UDC No. 551.553.21 : 551.52 (540.65)

Influence of sunspot activity and EL Niño southern oscillation on northeast monsoon rainfall in the coastal districts of Tamil Nadu

S. LAKSHMI, E.A.K. NIVETHAA*, K. PALANIVELU** and A. RAMACHANDRAN***

India Meteorological Department, Meteorological Training Institute, Pune – 411 021, Maharashtra, India

**Crescent Institute of Science and Technology, Department of Physics, Chennai – 600 048, Tamil Nadu, India*

***Centre for Climate Change and Environment, School of Civil Engineering,*

Vellore Institute of Technology, Chennai Campus, Chennai – 600 127, Tamil Nadu, India

****Center for Climate Change and Disaster Management, Department of Civil Engineering,*

Anna University, Chennai– 600 025, Tamil Nadu, India

(*Received 8 March 2024, Accepted 3 March 2025*)

e mals : lakshmiphy2@gmail.com; nivethaaeak3@gmail.com; k.palanivelu@vit.ac.in; andimuthu.ramachandran@gmail.com

सार – **वर्तमान अध्ययन** 1901-2020 **से भारत के तमिलनाडु (सीडीटीएन) के तटीय जिलों में स्थानीय पैरामीटर, उत्तर पूर्व मानसून वर्षा (एनईएमआर) पर सनस्पॉट नंबर (एसएसएन) और अल नीनो दक्षिणी दोलन (ईएनएसओ) जैसे वैश्विक चर के प्रभावों को स्थापित करने पर केंद्रित है। सौर चक्र के बढ़ते क्षेत्र में, न्यूनतम एसएसएन के वर्ष से लगभग दो वर्षों के भीतर अतिरिक्त वर्षा देखी जाती है। सौर चक्र और वर्षा (आरएफ) में सौर अधिकतम का** 1-4 **वर्ष का चरण विलंब (सौर चक्र लीड) होता है। फूरियर ट्रांसफॉर्मेशन और क्रॉस-सहसंबंध का उपयोग करके क्रमशः एसएसएन और वर्षा की आवधिकता और चरण विलंब की पहचान की गई है। सौर अधिकतम के के दौरान, वर्षा कम होती देखी गई है। प्राप्त परिणाम सौर अधिकतम और एनईएमआर के बीच व्युत्क्रम संबंध को स्पष्ट करते हैं सहसंबंध मानचित्र दो लगातार एल नीनो/ला नीना वर्षों में ओएलआर और अधिक/कमी वाले एनईएमआर वर्षों के संयोजन का विश्लेषण करता है। यह विश्लेषण पुष्टि करता है कि लंबे समय तक एल नीनो की घटनाओं के कारण अधिक वर्षा होती है, जबकि ला नीना की घटनाओं के कारण वर्षा में कमी होती है।** SSN, ENSO ENSO **और** NEMR **चक्रों के बीच अस्थायी संबंध की जांच करने के लिए मोर्लेट वेवलेट ट्रांसफॉर्मेशन** (MWT) **विश्लेषण का उपयोग किया गया है। इस अध्ययन के निष्कर्ष सनस्पॉट गतिविधिके आधार पर भविष्य के सूखे और गीले वर्षों की भविष्यवाणी करने और जल संसाधनों के बेहतर प्रबंधन के लिए नीति निर्माताओं के लिए उपयोगी हो सकते हैं।**

ABSTRACT. The current study is focused on establishing the effects of global variables such as the Sunspot Number (SSN)and El Niño Southern Oscillation (ENSO) on the local parameter, North East Monsoon Rainfall (NEMR) in the coastal districts of Tamil Nadu (CDTN) India from 1901-2020. In the rising region of the solar cycle, excess precipitation is observed within about two years from the year of minimum SSN. The solar cycle and rainfall (RF) have a 1-4year phase delay (solar cycle leads) of solar maximum. The periodicity and phase delay of SSN and precipitation have been identified using Fourier Transformation and cross-correlation, respectively. During the solar maximum, the precipitation is observed to be less. The obtained results elucidate the inverse relationship between solar maximum and NEMR as well as the invariance of NEMR during solar minimum. El Niño/La Niña and the sunspots maximum/minimum number have a high likelihood of co-occurring. The correlation map analyzes the composite of OLR and excess/deficit NEMR years across two consecutive El Niño/La Niña years. This analysis confirms that prolonged El Niño events lead to excess rainfall, while La Niña events result in rainfall deficit.The Morlet wavelet transformation(MWT) analysis has been used to examine the temporal connection between SSN, ENSO, and NEMR cyclicities. The findings of this study may be useful in predicting future droughts and wet years based on sunspot activity and to the policymakers for better management of water resources.

Key words – North East Monsoon, Sunspot Number, ENSO, Coastal districts of Tamil Nadu.

1. Introduction

The impact of the solar cycle on climate is significant in evaluating and differentiating between natural variability of climate and induced climatic changes. Thus, the inadequate understanding of the physical mechanisms of the atmosphere with solar activity is a significant issue (Chiodo *et al*., 2012) as solar energy steers the Earth's climate system and directly influences the climate from the decadal to century-scale as reported by Eddy (1976). A solar radiation change of about 0.1% was observed during a solar cycle of 11 years, causing a radiative forcing of intensity around 0.2 -0.3 W/m^2 in total radiation. Even though, this forcing seems small, a notable change in the UV range (200-250nm) is observed in space measurements during solar maximum to minimum conditions (Lean *et al.*, 1997).

The fluctuation in climate due to variation in solar activity can be discussed using Total solar irradiation(TSI), the spectrally integrated shortwave energy flux density in W/m^2 reaching the top of the atmosphere (Fedorov, 2019). The records show an 11-year oscillation of about $1W/m^2$ called the 11-year solar cycle. Strong fluctuation in TSI is also possible during shorter time scales. The solar cycle (SC) can be ascertained as the sunspot cycle. A Sunspot number (SSN) variation of about 100-200 units is observed during the peaks of SC. This increase curtails the visible light emitted by the Sun. TSI and sunspots (ringed brighter zones called 'faculae' that are obvious at extreme ultraviolet images of the Sun) are highly correlated on decadal time scales (Chiodo *et al.*, 2012).

Likewise, Solar activity (SA) is also associated with geomagnetic activity and galactic cosmic rays phenomena. An interrelation exists between the Sun, cosmic rays and rainfall (RF) worldwide (Svensmark *et al*., 2009). The descending phase of 11year SC usually coincides with the peak of galactic cosmic rays and is also associated with the geomagnetic storms. Similarly, SA and RF are also interlinked.

Northeast monsoon (NEM) season (October to December) is the principal rainy season for the southern region of the Indian peninsula, particularly the eastern half of it. In the state of Tamil Nadu, it is the primary rainy season which accounts for about 60% of the annual RF in the coastal districts and about 40% to 50% of the annual RF in the interior districts of the state. Hiremath and Mandi (2004) and Hiremath (2006) found that Indian RF is correlated with sunspot activity, and the occurrence of RF is high whenever there is high sunspot activity. The Sun is not only the source of energetic particles that penetrate the Earth's atmosphere but also the Galactic cosmic rays (GCR), which are mostly protons and alpha particles, have typically higher energies but lower fluxes than the solar cosmic rays. The most impressive modulation is the 11-year variation that shows a clear anti-correlation with the 11-year solar cycle, Bazilevskaya (2000) reported. Usoskin and Kovaltsov (2008) discussed a possible link connecting solar activity and climate variations to cosmic rays and the physical-chemical changes they produce in the atmosphere. Therefore, it is essential to study the influence on precipitation due to solar energetic particles and galactic cosmic rays.

During periods of intense solar activity, the Hadley circulation expands, causing a northward shift of the subtropical arid regions and the northern boundary of the monsoon. Consequently, this shift results in increased precipitation across various land areas (Haigh *et al*., 2005; Zhao *et al*., 2012). The relationship between sunspot number and average monthly precipitation has been documented and analyzed, revealing a significant correlation between solar activity and monthly average precipitation for specific months and time lags (Nitka and Burnecki, 2019). Previous studies have indicated that during solar maxima, precipitation increases over low-latitude land surfaces, decreases at mid-latitudes (20° to 40°) and then rises again at high latitudes (40°) (Wang *et al.*, 2005). Furthermore, sea surface temperature patterns associated with the 11-year solar cycle resembles those observed during El Niño/Southern Oscillation cold events (La Niña) (Gray *et al*., 2010). Zhai, 2017 has investigated the relationship between solar activity and precipitation in north-central China.

El Niño Southern Oscillation (ENSO) is identified as the most significant mode of interannual variability in the International and local weather systems, with a recurrence period around the 2-8 year band (Mendi, 2015; Santos, 2006). ENSO is a combination of the El Niño and southern oscillation, characterized by means of an interannual see-saw in tropical sea level pressure between the western and eastern Pacific, consisting of weakening and strengthening of the easterly trade winds over the tropical pacific (Sreekala *et al*., 2012; Vengateswari *et al*., 2019; Yadav, 2012). The relationship between monthly sunspot number and ENSO data for two periods (1996-2009 and 1950-2014) has been analysed by Hassan *et al*., (2016a).Several studies have observed a significant regional response to the 11-year solar cycle (SC). For instance, White *et al*. (1998) discovered that the SST variability associated with the 11-year solar cycle during the twentieth century closely resembled the spatial pattern of ENSO.Zhai (2017) has also explored the impact of solar activity on ENSO, using the El Niño index for the region defined as area 3 (5°S to 5°N, 150°W to 90°W).

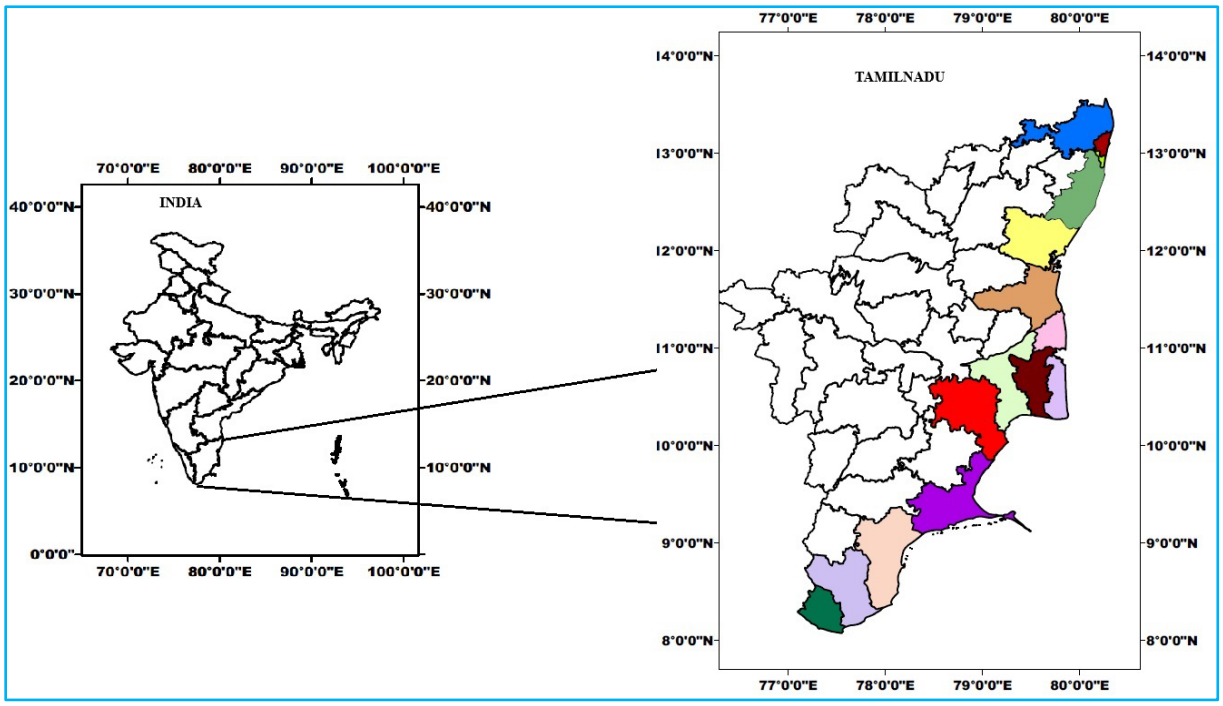

Fig. 1. Depiction of Coastal districts of Tamil Nadu state of South India

Historical records of El Niño events and sunspot number (SSN) have revealed an association between long-term changes in the solar cycle and the frequency of El Niño occurrences (Anderson, 1990).Increased total solar irradiance during periods of high solar activity tends to create conditions that favor the onset of the monsoon, resulting in greater precipitation in Southeast and South Asia before the peak of summer (July-August), despite ENSO-related patterns (Chen *et al*., 2024).Wang *et al*. (2021) has investigated the combined effects of ENSO and solar activity in mid-winter (January) SC using observational and reanalysis data. The study found that both ENSO and solar activity are positively correlated with SC, though they exhibit distinct spatial patterns.A study bySreekala *et al*. (2018), has highlighted the intricate interactions among El Niño, Indian Ocean Dipole (IOD), the Madden-Julian Oscillation (MJO) and monsoon dynamics, emphasizing the importance of a thorough investigation into these factors to better understand the behavior of Indian summer monsoon rainfall(ISMR).

ENSO's influence on the precipitation in the Coastal districts of Tamil Nadu (CDTN) India during NEM has already been established (Lakshmi *et al*., 2021). An important observation during this analysis was that the occurrence of El Niño over the CDTN was not the only reason behind the excessive RF, as there were a few discrepancies, which could be accounted for considering only the El Niño parameter. This led to the search and study of the other essential parameters like SSN and OLR. However, the dependence of precipitation on SSN has been reported (Hassan *et al*., 2016; Hiremath and Mandi, 2004). Not many reports account for excessive RF using ENSO, SSN and OLR, which is the energy emitted from the Earth's surface in the form of electromagnetic radiation that passes out of the atmosphere and into space as thermal radiation. The uniqueness of this work thus lies in relating these three parameters and explaining how they directly influence the RF pattern during NEM in CDTN.

The present study aims to analyze the effects of SC (in terms of SSN) and El Niño on the excessive precipitation observed in CDTN, as shown in Fig. 1, during the NEM season. This work thus will pave the way to give a broad picture of the RF pattern, which will prove to be helpful in agricultural crop production over south peninsular India as it is strongly influenced by the NEMR.

2. Data and methodology

2.1. *Data*

The current study used daily gridded RF data from the Indian Meteorological Department with a high spatial resolution (0.25 × 0.25 degree) from 1901 to 2020 (Pai *et al*., 2014).

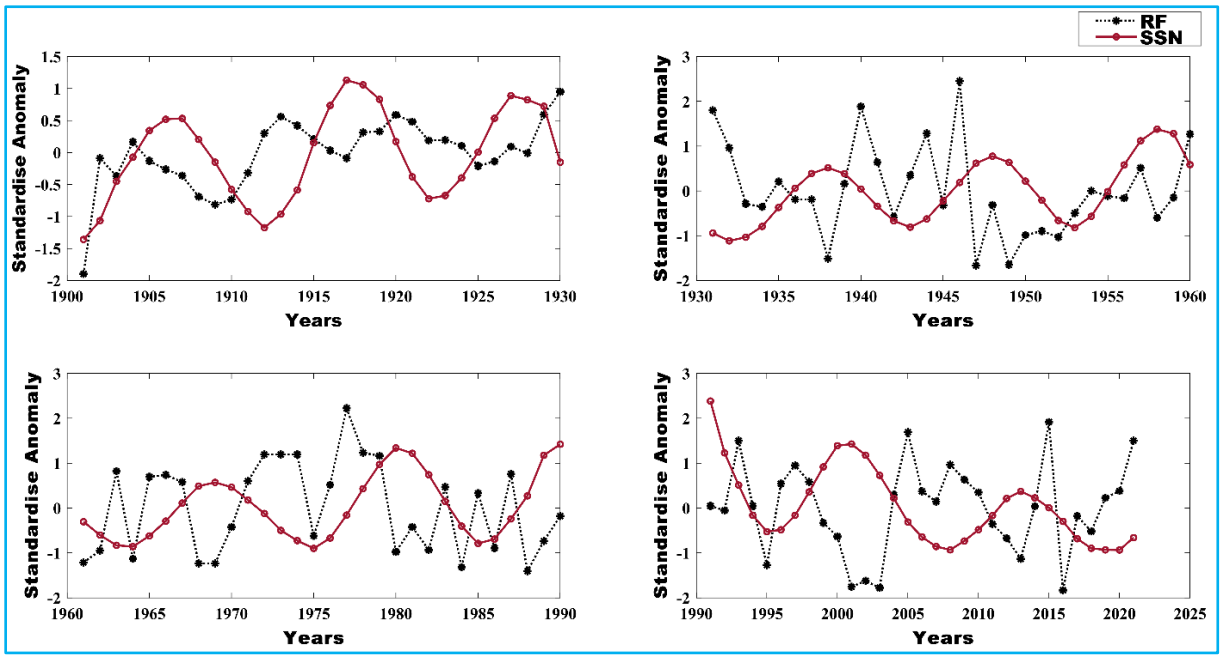

Fig. 2. Graph of Standardized anomaly of NEMR *vs.* SSN for climatological period and represents the absence of excessive rainfall during the year when the SSN reaches maximum

The ESAI website (http://www.gao.spb.ru/database/esai/) provided monthly and annual SSN for the same time interval as the data mentioned above.

The Nino 3.4 Sea Surface Temperature (SST) Index was calculated using the Met Office Hadley Centre Sea Ice and Sea Surface Temperature version 1.1 (HadISST1.1) (Rayner *et al.*, 2003). The HadISST1.1 dataset is available from 1950 to 2020 and has a resolution of 1.0° × 1.0°. It is available on the internet (www.esrl.noaa.gov/psd/gcoswgsp/Timeseries) and is the area-averaged SST from 5°N-5°S and 170°-120°W.

Outgoing Long-wave Radiation (OLR) data was obtained from the ERDDAP at the APDRC NOAA website and was measured by the Advanced Very High-Resolution Radiometer (AVHRR) onboard the NOAA Polar Orbiting satellites starting in 1974. The datasets utilized here cover the years 1974 to 2021 and are available on the internet. http://apdrc.soest.hawaii.edu/thredds/dodsC/las/olr_monthly/data_apdrc.soest.hawaii.edu_dods_public_data_satellite_product_OLR_olr_monthly.jnl.html.

The National Centers for Environmental Prediction (NCEP)/National Center for Atmospheric Research (NCAR) reanalysis data for surface 850hPa vector wind anomaly has been utilized to examine the circulation features. The synoptic features during the NEM season across the tropical region (20° S-20° N, 50-150° E) have been studied using data retrieved from the website www.cdc.noaa.gov.

2.2. *Methodology*

2.2.1. *Statistical analysis and trend detection*

To identify the climate pattern, the study period has been divided into four climatological periods, namely (1901-1930), (1931-1960), (1961-1990) and (1991-2020) for precipitation and (1901-1930), (1931-1960), (1961-1990) and (1991-2020) for SSN and El Niño index. The mean and standard deviations have been used to calculate the

$$\text{Standardised anomaly} = \frac{x - \mu}{\sigma} \qquad (1)$$

The standardized anomaly has been calculated for precipitation, Oceanic Nino Index (ONI) and SSN. To understand the long-term influence of solar activity on RF variability, the plots of the standardized anomaly of SSN and RF for the climatological periods (1901-1930), (1931-1960), (1961-1990) and (1991-2020) are shown in Fig. 2. When the difference between the October to December (OND) precipitation and climatological period precipitation mean value is more than the triple, double mean square deviations are called extreme, and if it is less

than triple, then the double mean square deviations are called deficit precipitation.

Cross-correlation analysis (CCA) is a well-known approach for determining the similarity between two signals. Many authors have utilised this strategy (Adhikari *et al*., 2018; Poudel *et al*., 2019; Tsurutani *et al*., 1990). The classical correlation has been determined by the displacement of one series relative to the other in time (t) units, which gives the correlation's lag (Boyd, 2001).

Correlation formula.

$$\$_{pi,j} = \frac{\sum_{t=1}^{N} \left[\left(x_i^t - \overline{x}_i\right)\left(x_j^t - \overline{x_j}\right)\right]}{\sqrt{\sum_{t=1}^{N} \left(x_i - \overline{x}_i\right)^2 \left(x_j - \overline{x_j}\right)^2}} \quad (2)$$

To identify the phase difference between the NEMR and SSN, Years 1901-2020 divided into 12 decades, and the cross-correlation for each has been applied. The relation between RF and maximum SSN has then been studied. Regional precipitation anomalies, floods, and other disasters have good response linkages to solar activity, global climatic anomalies, atmospheric circulation and El Niño events (Prestes *et al*., 2006).

2.2.2. *Wavelet transformation*

In order to obtain additional information from a signal, which is unavailable in its raw form, mathematical transformations are used. Of these, the windowed Fourier transformation is the most well-known one. Although this method solves the problem of frequency localization, it is subject to the window size employed and its being based on the supposition that the signal can be split into sinusoidal components. These drawbacks are overcome by using Wavelet Transformation (WT), wherein a 1-D time series is converted into a diffuse 2-D time-frequency image (Banu *et al*., 2015). So this method is based on collecting the amplitude of a periodic signal and studying its variation over time. To compute the variance, the Morlet wavelet shape having a specific period was used as a window function. The Morlet wavelet consists of a plane wave modulated by Gaussian (Augusto and Santos, 2016; Torrence and Compo, 1998).

$$\Psi_0(\eta) = \pi^{-\frac{1}{4}} e^{i\omega_0\eta} e^{\frac{-\eta^2}{2}} \quad (3)$$

where $\psi_0(\eta)$ is wavelet at non-dimensional time η and ω_0 is the non-dimensional frequency, which is taken to be 6 here.

This is the basic wavelet function, but there is a need to change the overall size and slide the entire wavelet along in time. Thus, the "scaled wavelets" are defined as:

$$\Psi\left[\frac{(n'-n)\delta t}{s}\right] = \left(\frac{\delta t}{s}\right)\Psi_0\left[\frac{(n'-n)\delta t}{s}\right] \quad (4)$$

where

s = dilation parameter used to change the scale

n = translational parameter used to slide in time

$S^{-1/2}$ = normalization to keep the total energy of the scaled wavelet is constant

The continuous wavelet transform of a discrete sequence x_n is defined as the convolution of x_n with a scaled and translated version of $\psi_0(\eta)$

$$W_n(s) = \sum_{n=0}^{N-1} X_{n'} \Psi * \left[\frac{(n'-n)\delta t}{s}\right] \quad (5)$$

where * = complex conjugate

A picture showing both the amplitude of any features versus the scale along with the variation of amplitude with time can be obtained by varying the wavelet scale s and translating along with the localized time index *n*. The subscript 0 on ψ has been dropped to indicate that this ψ has also been normalized. However, it is possible to calculate the wavelet transform using Eqn. (2), it is considerably faster to do the calculations in Fourier space. By the convolution theorem, the wavelet transform is the inverse Fourier transform of the product:

$$W_n(s) = \sum_{k=0}^{N-1} \$\, \psi^*(s\omega_k) e^{i\omega_k n\delta t} \quad (6)$$

Where ω_k is the angular frequency equal to $2\pi k$ / $N\delta t$ for $k \leq N/2$ or equal to $-2\pi k$ / $N\delta t$ for $k > N/2$. It is possible to compute the wavelet transform in the time domain using Eqn. (3). Hence, this study employed the Morlet wavelet to explore the variation and periodicity of precipitation, SSN, and ENSO.

In this study, wavelet analysis was employed to deconstruct the original data and explore the periodic variations in Sunspot Number (SSN), precipitation, and the El Niño index. Specifically, we used the Morlet wavelet transformation, which is well-suited for analyzing non-stationary time series due to its ability to capture both

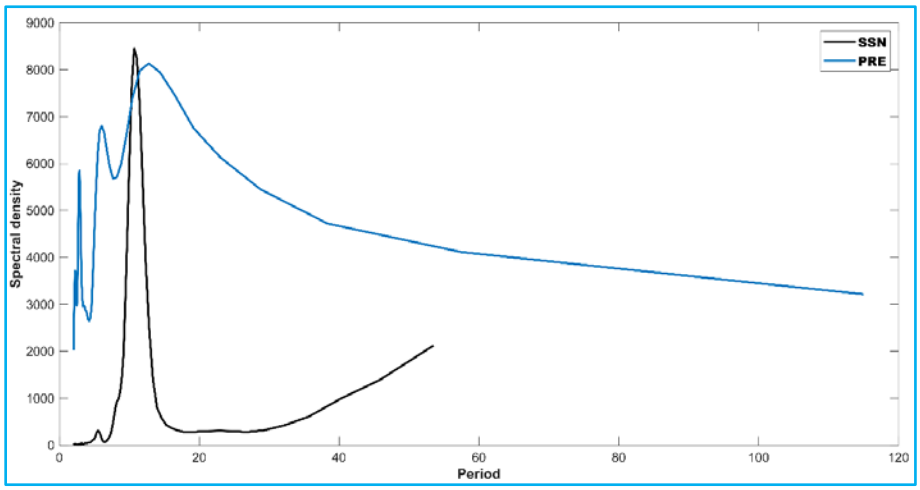

Fig. 3. Depiction of Fourier spectral density variation of SSN with NEMR

temporal and frequency information. To visualize these analyses, we have utilized the MATLAB software to generate Wavelet Coefficient Contour Maps of the precipitation time series across a 64-year scale.The 64-year scale is often selected to capture long-term oscillatory patterns and cycles that may be present in the data. For example, sunspot cycles, certain climatic patterns and ENSO phenomena can exhibit multi-decadal variability. A 64-year scale helps in identifying and analyzing these long-term cycles and trends effectively. Morlet wavelets provide a balance between time and frequency resolution. Choosing a scale of 64 years allows for sufficient resolution to analyze low-frequency components of the data, while still capturing significant long-term oscillations. This is particularly useful for studying phenomena that exhibit cycles longer than a single decade but shorter than a century. The length of the time series data available often dictates the choice of wavelet scales. For time series that span several decades to over a century such as SSN, precipitation and ENSO data, a 64-year scale is suitable for analyzing significant historical patterns and trends without being overly influenced by short-term fluctuations.

To handle anomalies and outliers, we first applied a preprocessing step involving robust filtering to reduce their impact on the wavelet transformation. We identified and addressed outliers using Z-score thresholds ensuring that these extreme values did not unduly influence our analysis. The Morlet wavelet scales were selected based on known periodicities. The Morlet wavelet's scales were carefully chosen to balance time and frequency resolution, allowing us to accurately capture the oscillatory patterns and trends within the data. We conducted Morlet Wavelet Transformation (MWT) on SSN, ENSO and precipitation (RF) series to analyze their temporal and spectral characteristics. The choice of scales and the handling of anomalies were crucial in ensuring the robustness and reliability of our results.

Additionally, we acknowledge the limitations of wavelet transformation analysis. One notable limitation is that wavelet analysis may be sensitive to the choice of scales and the specific wavelet function used, which can affect the interpretability of the results. Moreover, wavelet analysis may not fully capture non-stationary phenomena if the chosen scales do not align well with the data's inherent frequencies.

Finally, based on the availability of OLR data years, the excess and deficit NEMR years from 1974 to 2015 are determined from precipitation anomalies. The influence of OLR on precipitation and its correlation with the excessive RF years (consecutive El Niño years) as well as deficit RF years (consecutive La Niña years) from our previous study (Lakshmi *et al.*, 2021) has been established using composite analysis done using Arc Map 10.5. The wind pattern has also been analyzed for these specific periods.

3. Results and discussion

3.1. *Statistical analysis*

Annual RF in the CDTN is non-stationary and nonlinear from 1901 to 2020, with no discernible periodic fluctuation (Fig. 2). Fig. 2 shows the plot of the standardized anomaly of NEMR vs. SSN for the climatological period. The graph shows that there is no excessive RF during the year when the SSN is at its maximum. The peaks denoting excessive RF are majorly observed to coincide with the ascending portion of the

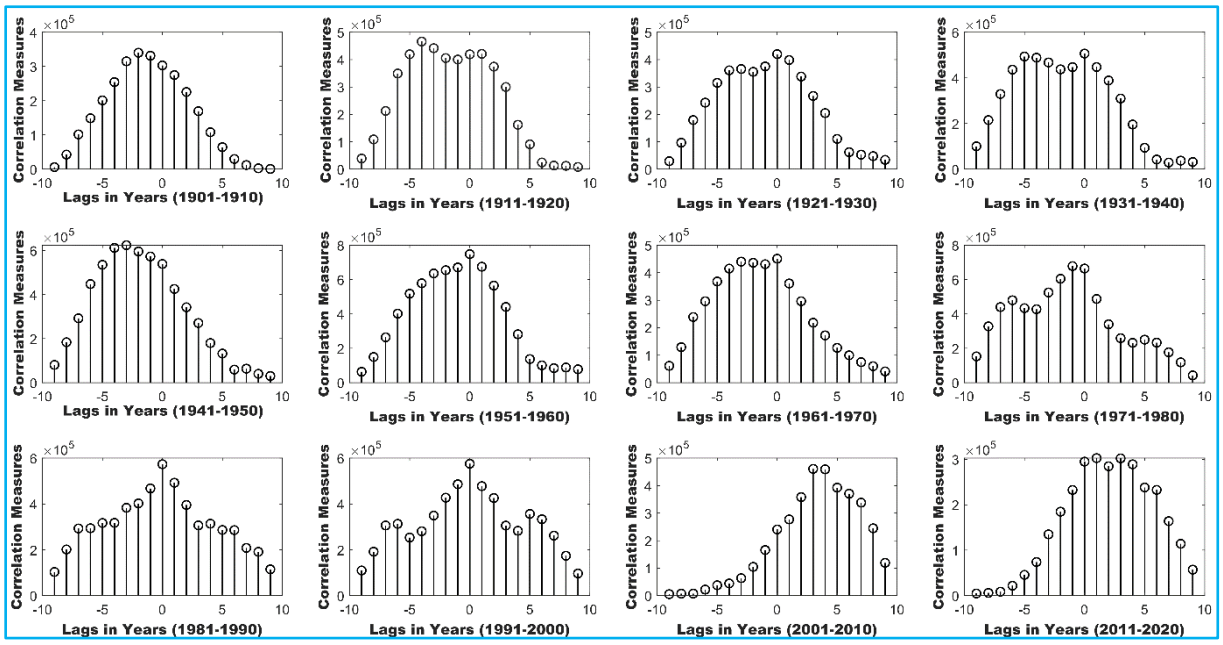

Fig. 4. Cross-correlation between the SSN and NEMR to determine the phase delay. The '0' in the graph shows the maximum SSN during the specific decade. The year of occurrence of RF maximum has been counted starting from this

TABLE 1

Maximum and Minimum years of Sunspot number during excess and deficit NEMR - Excessive rainfall is prevalent only during the 2 years in close proximity to the minimum SSN and a period of about 4 years before reaching the maximum SSN

Maximum Sunspot No.		Minimum Sunspot No.		Excess RF Year	Excess RF anomaly mm
Year	RF anomaly mm	Year	RF anomaly mm		
1905	-57.02	1901	313.43	1902	313.43
1917	-132.65	1913	306.27	1914	262.26
1928	88.72	1923	14.69	1925	299.06
1937	-67.05	1933	-84.62	-	-
1947	-336.4	1944	201.29	1946	413.83
1957	60.73	1954	-32.09	-	-
1968	-184.95	1964	-168.52	1966	126.39
1979	193.16	1976	91.35	1977	360.39
1989	-106.08	1986	-131.49	1987	129.37
2000	-119.88	1996	148.89	1997	242.67
2014	33.75	2008	246.13	2010	104.41
		2019	75.65		

curve where the SSN is increasing towards reaching the maximum value. The precipitation pattern in the CDTN area and the SSN were consistent compared to the precipitation and SSN statistics. Through a correlative estimate with a significance test, the long-term influence of SSN on seasonal and annual RF variability is investigated. The significance level has been set at 95% (*p*-value 0.05).

The observed shift in the spectral density of SSN as compared to that of the spectral density of NEMR determined *via* Fourier analysis (Fig. 3), is affirmative of

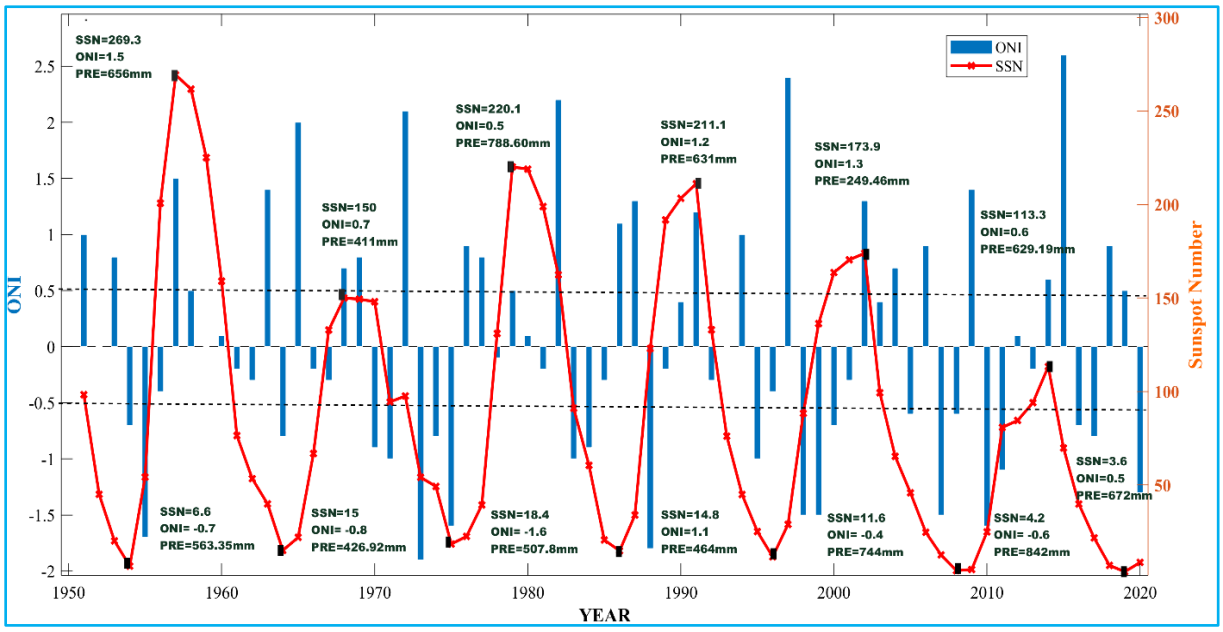

Fig. 5. Variation of SSN and ENSO (The Black horizontal lines represent the NOAA operational definition of El Niño and La Niña. ONI greater than or equal to 0.5 represents an El Niño year and ONI less than or equal to -0.5 depicts La Niña years)

the influence of the solar cycle on the RF variability (Bhattacharya, 2014; Bhattacharyya and Narasimha, 2005; Chaudhuri *et al*., 2015; Zhao *et al*., 2012). The mismatch in the peaks of NEMR and SSN clearly substantiates the results of the previous plot(Fig.2).

The graph of SSN *vs*. RF for several decades has been generated using cross correlation statistics, as shown in Fig. 4. The obtained results clearly indicate the occurrence of RF can happen either during the four successive or 4 preceding years from the year of occurrence of maximum SSN. The '0' in the graph shows the maximum SSN during the specific decade. The year of occurrence of RF maximum has been counted starting from this can be performed using Eqn. 2. The cross-correlation output on RF and the solar cycle shows that excessive RF occurs significant only when the SSN goes from a minimum until it reaches the maximum. Within these years covered by the minimum to maximum zones, excessive RF is prevalent only during the 2 years in close proximity to the minimum SSN and about 4 years before reaching the maximum SSN (Table 1). Our study reveals a notable lag between solar maximum periods and excess precipitation in the Northeast Monsoon of Tamil Nadu's coastal districts. This finding is consistent with similar patterns observed in other regional studies. Specifically, the same kind of lagging between precipitation and the solar cycle has been documented in various studies conducted across different regions (Alamoudi *et al*., 2023; Laurenz *et al*., 2019; Nazari-Sharabian and Karakouzian, 2020; Szypcio and Dolzyk-Szypcio, 2019; Zhao *et al*., 2012).

The noteworthy observation from Fig. 5 of SSN *vs* NEMR, a decrease in NEM RF is observed during the 11 solar maximum from 1901 to 2020. The solar maximum years with less precipitation anomalies from 1901-2020 years are 1905(-57.02mm), 1917(-132.65mm), 1928(88.72mm), 1937(-67.05mm), 1947(-336.4mm), 1957(60.73 mm), 1968(-184.95mm), 1979(193.16mm), 1989(-106.08mm), 2000(-119.88mm), 2014(33.75mm)are given in Table 1. In our study, we observed that during periods of solar maximum, there was a tendency for reduced precipitation in the specific context of the Northeast Monsoon in Tamil Nadu's coastal districts. This finding aligns with certain regional studies but may differ from global or generalized patterns(Gachari *et al*., 2014; Laurenz *et al*., 2019). The reduction in NEMR is attributed to the highly charged particles being emitted from the solar surface during periods of increasing solar activity. The Sun emits more UV and visible radiation, causing a reduction in the intensity of the GCR flux (Cliver, 2001; Forbush, 1954). This consequently slows down the nucleation of cloud particles, leading to a reduction in RF (Parker, 1999). The same is also explained in the cosmic-ray-cloud-climate hypothesis explained by other researchers (Hiremath, 2006; Jon Egill Kristjansson and Jorn Kristiansen, 2000) as follows: greater solar activity reduces cosmic ray flux, which reduces cloud cover, resulting in weaker cloud forcing and

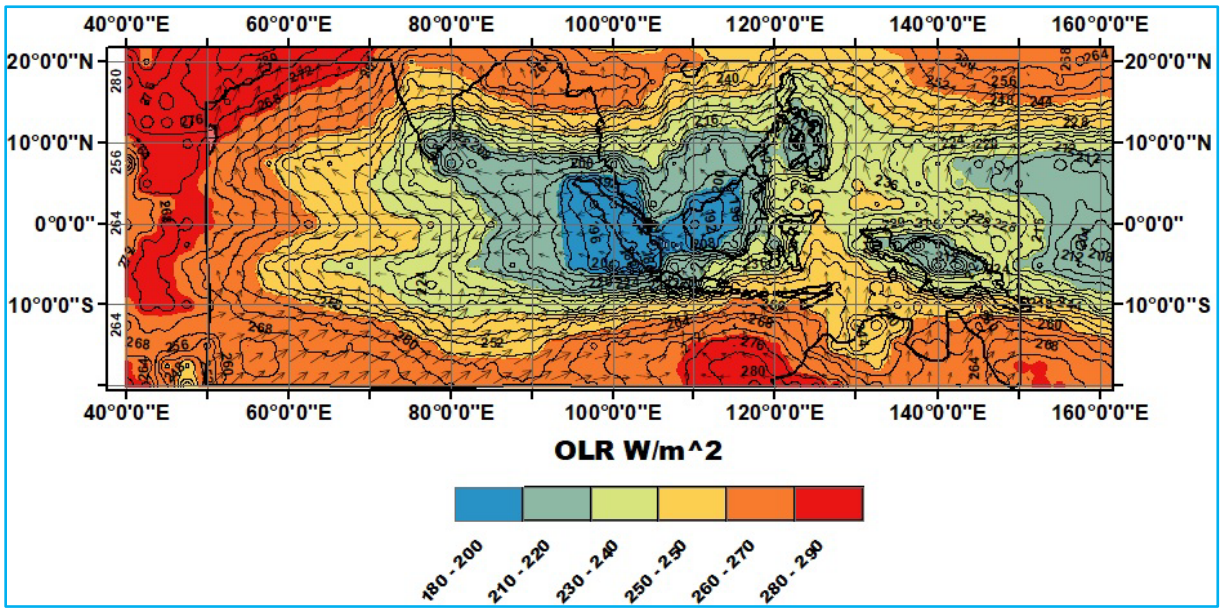

Fig. 6. Composite analysis of wind-Outgoing Longwave Radiation (OLR) during the Excessive rainfall (Consecutive El Niño) years of NEM season for the period from 1974-2015

TABLE 2

Relationship between Sunspot number and ENSO

Maximum Sunspot year	ENSO	Minimum Sunspot year	ENSO
1957	Strong El Niño	1954	La Niña
1968	El Niño	1964	La Niña
1979	El Niño	1975	La Niña
1989	Neutral	1986	El Niño
2000	Weak La Niña	1996	Weak La Niña
2014	El Niño	2008	La Niña
		2019	El Niño

a warmer temperature (Chaudhuri *et al*., 2015). So, the cosmic rays colliding with interplanetary magnetic fields behave like a shield against cosmic rays during high solar activity (Usoskin, 2005). The solar minimum values from 1901 to 2015 are not significantly correlated with precipitation.

The correlation between ENSO and SSN has also been established in this study. It is observed that El Niño (La Niña) years corresponded with solar maximum (solar minimum) as given in Table 2 and shown in Fig. 5. The positive correlation between ENSO and NEMR has been established previously (Kripalani and Kumar, 2004; Kumar *et al*., 2007; Lakshmi *et al*., 2021; Rajeevan *et al*., 2012; Yadav, 2012; Zubair and Ropelewski, 2006). Our previous report (Lakshmi *et al*., 2021) clearly evidences the positive correlation between ENSO and NEMR in CDTN, *i.e*., NEMR is more in CDTN during consecutive El-Nino years and less during consecutive La-Nina years. However, in our study on the relationship between ENSO and NEMR, contradictory results were also observed during a few years wherein excessive RF was absent even during the prevalence of consecutive El Niño events and deficit RF was absent during the occurrence of consecutive La Nin events. These odd results are satisfactorily explained in this work by correlating SSN and NEMR. However, in our study on the relationship between ENSO and NEMR, contradictory results were also observed during a few years. In general, the occurrence of El Niño for two successive causes excessive RF or flooding, whereas, the prevalence of consecutive La Niña events leads to deficit RF or drought. Still, there are a few years which do not fall under this trend. These odd results are satisfactorily explained in this work by correlating SSN and NEMR. The obtained results show that deficit RF occurs during strong/successive El Niño events if the sunspot number is maximum. This is attributed to the maximum solar activity when the SSN is maximum, resulting in a decrease in GCR flux intensity. Thus, the cosmic rays colliding with the interplanetary magnetic field act as a shield, which prevents the cosmic rays from entering the Earth, consequently impeding, cloud nucleation. Likewise, the occurrence of RFin spite of the occurrence of consecutive La Niñaevents (*e.g*., 2008) is ascribed to the sunspot number being minimum

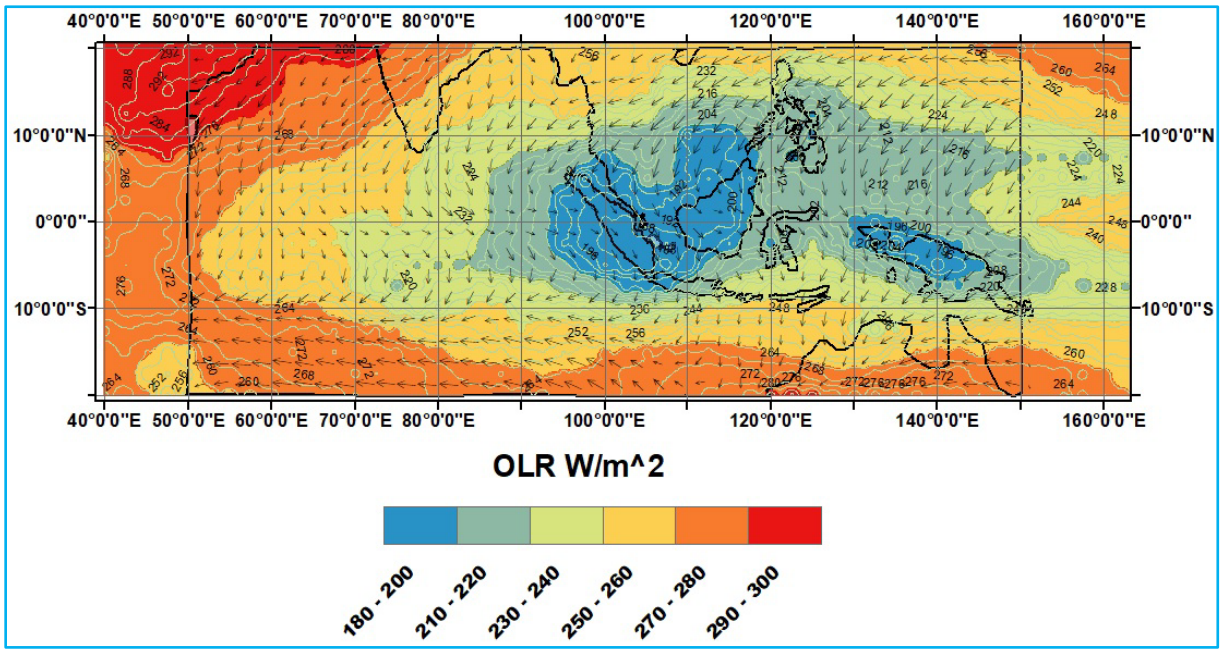

Fig. 7. Composite analysis of wind-Outgoing Longwave Radiation (OLR) during the deficit rainfall (Consecutive La Niña) years of NEM season for the period from 1974-2015

wherein the solar activity is minimum, facilitating cloud nucleation and thus causing more RF.

3.2. *Impacts of OLR on NEM*

OLR is the total amount of thermal radiation emitted from the Earth to interplanetary space. OLR has in general, been used to simulate RF. The dry spell is represented by a high OLR value, whereas the wet spell is represented by a low OLR value, as shown in Fig. 6 and 7. Fig. 6 and Fig. 7 illustrate the composite analysis for the same prolonged El Niño and La Niña years and OLR.In our analysis, we observed that consecutive El Niño years are associated with excess rainfall, while consecutive La Niña years tend to result in deficit rainfall. OLR data provides valuable support for these findings. Specifically, during consecutive El Niño years, lower OLR values were observed, indicative of increased cloud cover and convective activity, which correlates with the observed excess rainfall. Conversely, during consecutive La Niña years, higher OLR values were recorded, reflecting reduced cloudiness and suppressed convection, consistent with the observed rainfall deficits. The intensified convection over the Indian subcontinent and toned-down convection over the south Indian Ocean, during the excess monsoon years under low OLR is ascribed to the southerly and southeasterly wind at 850 hPa levels over the Indian region and surroundings. During this period, south easterlies from the Bay of Bengal and Indian Ocean region to the Indian subcontinent bring more moisture towards south peninsular India, thereby boosting the amount of RF over this region. Anomalous easterlies over the equatorial Indian Ocean are associated with excess monsoon years. This highlights the role of El Niño events in causing excess RF during the NEM season under low OLR and La Niña events in driving deficit RF during NEM under high OLR. The substantial link between OLR and ENSO is evident from the obtained results. The occurrence of El Niño is strongly related to low OLR and that of La Niña is associated with high OLR.

3.3. *Wavelet analysis of SSN, ENSO and NEM*

Since the 1980s, the WT has been a significant advancement in the field of data analysis. WT is a powerful tool for dealing with time-series data, particularly those with non-stationary characteristics. CDTN experiencing high climate extremities during the past decades showed no discernible periodic variation. SSN, on the other hand, displayed a clear period. The SSN was employed in this study to analyze solar activity. The precipitation pattern in the CDTN and the SSNwas consistent compared to the precipitation and SSN statistics. The wavelet amplitude and phase are shown to create a two-dimensional image of the variability. A mother wavelet can then be used to decompose a time series into time-frequency phase space. An algorithm to calculate the wavelet transform has already been reported

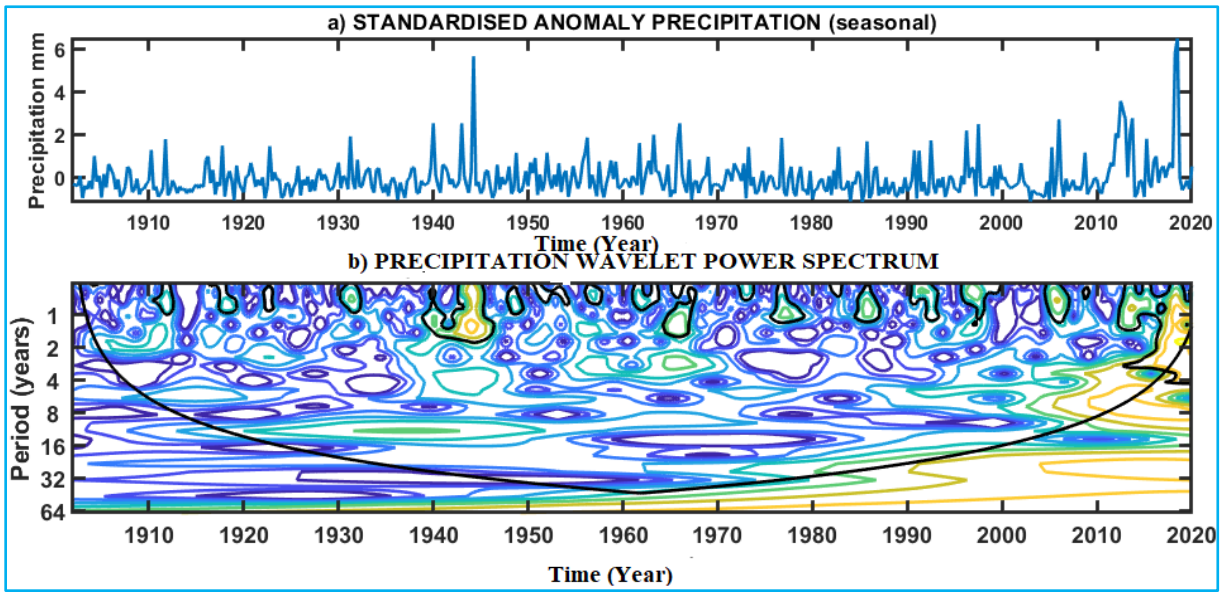

Figs. 8(a&b). (a) Depiction of standardized anomaly of NEMR. (b) NEMR wavelet power spectrum (1901-2020); crosshatched sections on either end illustrate the cone of influence

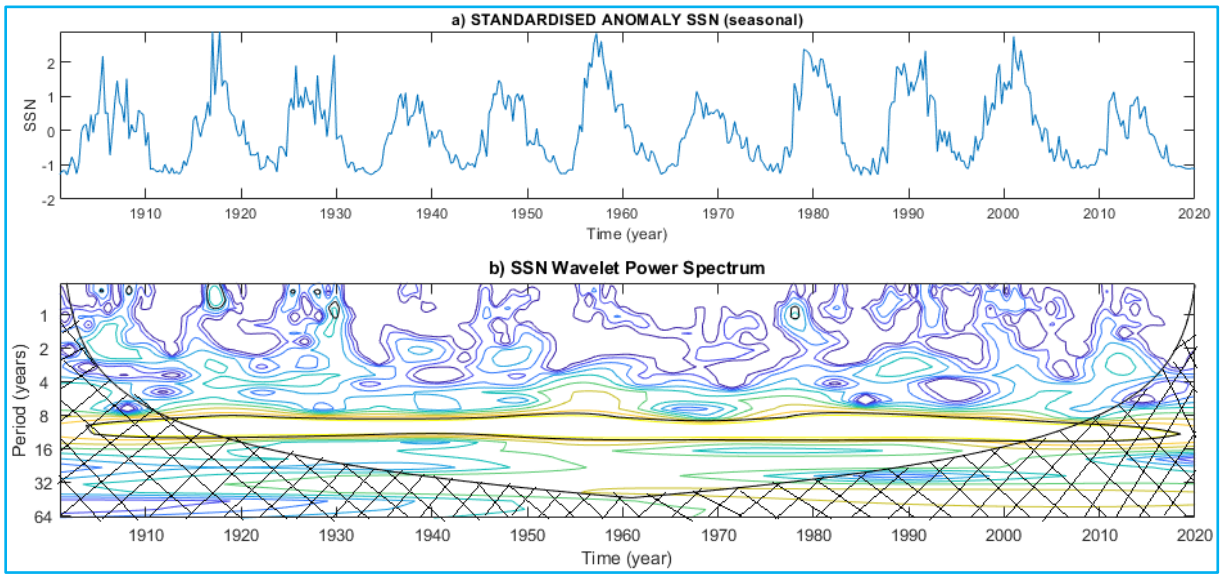

Figs. 9(a&b). (a) Depiction of standardized anomaly of SSN. (b) Sunspot numbers (SSN) wavelet power spectrum (1901-2020); crosshatched sections on either end illustrate the cone of influence

(Torrence and Compo, 1998). The wavelet analysis method has been used to decompose the original data and analyze the period of SSN, precipitation and ENSO.

The parameters used in the wavelet analysis are δt = 0.25 year and s0 = 2 Years because s = 2t; δj = 0.25 to do 4 sub-octaves per octave; and $j1$ = 7/δj to do 7 powers-of-two with δj sub-octaves each. Higher precipitation is represented by the red zone, lower precipitation is represented by the blue zone and middle precipitation is represented by the other hues. For a red-noise process with a lag-1 coefficient of 0.72, the thick black contour encloses regions of greater than 95% confidence. The "cone of influence" is indicated by cross-hatched zones on both ends. Fig. 8(a) (top) shows the NEMR seasonal standardized anomaly time series, Fig. 8(b) (bottom) displays the wavelet transform's power for the NEM seasonal RF in CDTN, which is a recordfrom 1901 to 2020. The power in the 1-3 year RF band depicts dry and wet years, with a significant decrease in power indicating a dry year and a significant increase in power indicating a wet year. The wavelet spectrum of SSNs for

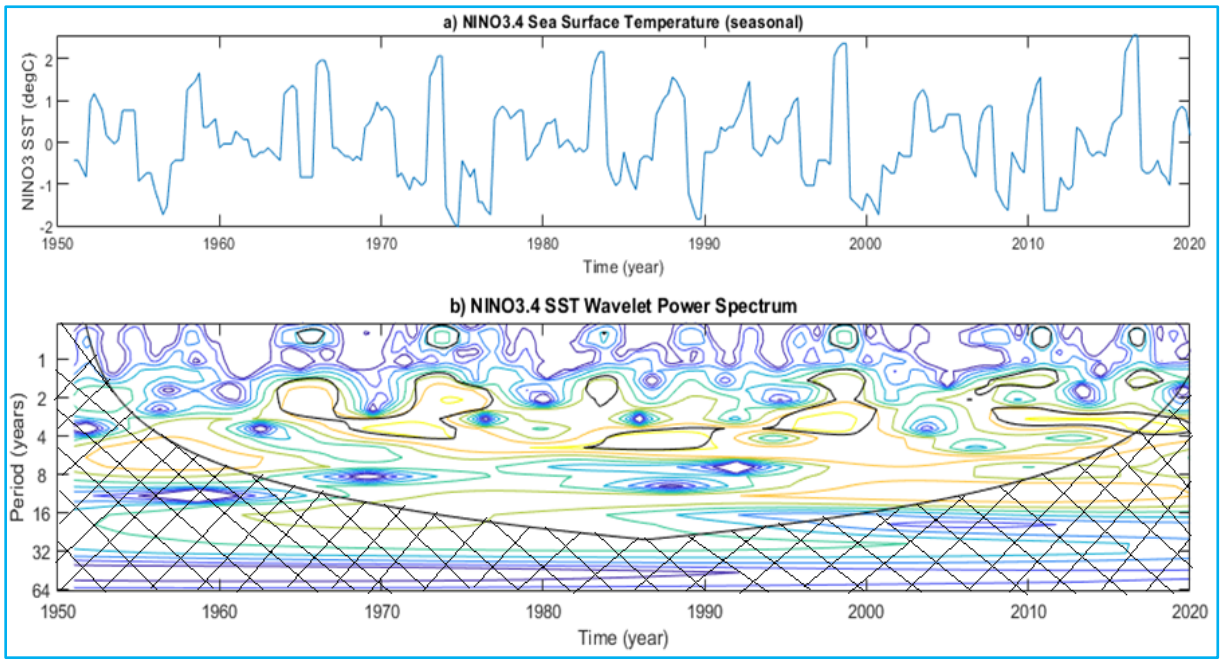

Figs. 10(a&b). (a) Depiction of standardized anomaly of ENSO. (b) ONI for Nino 3.4 SST wavelet power spectrum (1901-2020); crosshatched sections on either end illustrate the cone of influence

the considered period, indicates prominent phases between 9 and 11 years (Hiremath, 2006; Hiremath and Mandi, 2004). Fig. 9(a) shows that the signal at 11 years is the strongest and persists throughout the series, showing that the sunspot time series is non-stationary.The correlation between the highest points in the wavelet spectrum and the peak of sunspot activity is clearly observed [Fig. 9(b)]. The signal is non-stationary, and sways periodically from being present to being absent. Fig. 10(a)(top) shows the NINO3.4 index's seasonal standardized anomaly time series and Fig. 10(b) (bottom) shows its MWT power spectrum (bottom). Periodicity (inverse of frequency) is shown in the vertical axis of the wavelet power spectrum plot, and the horizontal axis indicates the time from 1950 to 2020. The clustering of the majority of the higher wavelet powers of the Nino 3.4 is prominent in periodicities of 2 to 6 years. However, the Nino 3.4's average amplitude and dominant mode before 2000 and after 2000 are entirely different from one another. The period of increased Nino 3.4 wavelet power is in good agreement with high precipitation wavelet power and vice versa. The smaller amplitude cycles seen at the 1 to 3-year periodicity of precipitation match the 2 to 3-year periodicity of Nino 3.4.

4. Conclusion

El Niño as a single parameter is insufficient to explain the RF pattern observed during NEM in the CDTN from 1901 to 2020. This study encompassing the analysis of other parameters like SSN and OLR has proven to give a better insight into the causes of extremities during NEMR in CDTN, which further enable interpretation of the future RF pattern. Changes in NEMR are observed only during the rising (upward trend) region of the solar cycle. In specific, excessive RF happens either within 2 years from SSN minimum or within a period of 4 years before reaching SSN maximum. In contrast, the descending(downward trend in SC) region does not show any such pattern in precipitation.These findings challenge existing models of solar influence on precipitation and suggest that the relationship may be more nuanced than a straightforward correlation. This discrepancy highlights the need for further investigation into the mechanisms behind this lag and how regional factors might modulate solar effects on precipitation.To address these issues, future research has to be focussed on : (*i*) Examining longer time series data to better understand the temporal dynamics of the solar cycle's impact on precipitation. (*ii*) Conducting similar studies in different climatic regions to see if the lag pattern observed in Tamil Nadu is present elsewhere. (*iii*) Investigating the underlying atmospheric and oceanic processes that could explain the observed lag and its variability across regions.

The solar maximum years exhibit less precipitation, while the minimum solar years do not have any significant impact on precipitation. All solar maximum years have the highest likelihood of El Niño, whereas all solar minimum years have the highest probability of La Niña.

A cogent explanation is available for mapping all the 3 parameters with NEMR even for the years where deficit RF is observed despite the persisting El Niño conditions and vice versa. So, theRF pattern from 1901 to 2020 has been precisely discerned and explained using the 3 parameters. In addition to the well-documented influence of ENSO on the Northeast Monsoon, it is important to recognize that other large-scale climatic phenomena, such as IOD and MJO, also play significant roles in shaping monsoon patterns. For instance, the year 2015 serves as a pertinent example: while it was predominantly characterized by a strong El Niño event, it was also marked by a positive IOD phase and notable MJO activity. This example underscores the complexity of climate interactions and highlights that while El Niño is a major driver of monsoon variability, other factors such as IOD and MJO must also be considered to fully understand and predict the behavior of the NEM.

Disclaimer : The contents and views presented in this research article/paper are the views of the authors and do not necessarily reflect the views of the organizations they belongs to.

References

Adhikari, B. Dahal, S. Sapkota, N. and Baruwal, P., 2018, "Earth and Space Science Field-Aligned Current and Polar Cap Potential and Geomagnetic Disturbances : A Review of Cross-Correlation Analysis". https://doi.org/10.1029/2018EA000392.

Alamoudi, H. A. Maghrabi, A. and Alruhaili, A., 2023, "Precipitation periodicities in Saudi Arabia and its possible link to solar activity", *ICRC2023*, p1258.

Anderson, R. Y., 1990, "Solar-Cycle Modulations of ENSO: A Possible Source of Climatic Change", In J. L. Betancourt and A.M. Mackay,editors, Proceedings of the sixth Annual Pacific Climate workshop, 77-81.

Augusto, C. and Santos, G., 2016, "Rainfall analysis in Klang river basin using continuous wavelet", *J. Urban Environ. Eng*., **10**, 1-9. https://doi.org/10.4090/juee.2016.v10n1.003010.

Banu, S. Guo, Y. Hu, W. Dale, P. Mackenzie, J. S. Mengersen, K. and Tong, S., 2015, "Impacts of El Niño Southern Oscillation and Indian Ocean Dipole on dengue incidence in Bangladesh", *Sci. Rep*., **5**, 1-9. https://doi.org/10.1038/srep16105.

Bazilevskaya, G. A., 2000, "Observations of variability in cosmic rays", *Space Sci. Rev*., **94**, 25-38. https://doi.org/10.1023/A:1026721912992.

Bhattacharya, A. B., 2014, "Sunspot Activity Over the Indian Rainfall Pattern", *IJECT*, **5**, 2-5.

Bhattacharyya, S. and Narasimha, R., 2005, "Possible association between Indian monsoon rainfall and solar activity", *Geophys. Res. Lett.*, **32**, 1-5. https://doi.org/10.1029/2004GL021044.

Boyd, D. W., 2001 "Stochastic Analysis, Systems Analysis and Modeling". https://doi.org/10.1016/b978-012121851-5/50008-3.

Chaudhuri, S. Pal, J. and Guhathakurta, S., 2015, "The influence of galactic cosmic ray on all India annual rainfall and temperature", *Adv. Sp. Res*.,**55**, 1158-1167. https://doi.org/10.1016/j.asr.2014.11.027.

Chen, P.J. Wu, C. H. Chen, Y. G. and Lee, S. Y., 2024, "Impact of Solar Activity and ENSO on the Early Summer Asian Monsoon During the Last Millennium", *Geophysical Research Letters*, **51**, 3, 1-10.

Chiodo, G. Calvo, N. Marsh, D.R. and Garcia-Herrera, R., 2012, "The 11-year solar cycle signal in transient simulations from the Whole Atmosphere Community Climate Model", *J. Geophys. Res. Atmos.*, **117**, 1-21. https://doi.org/10.1029/2011JD016393.

Cliver, E. W., 2001, "22 year patterns in the relationship of sunspot number and tilt angle to cosmic-ray intensity", *Astrophys. Force*, **551**, 189-192.

Eddy, J. A., 1976, "The maunder minimum", *Science*, **80**, 192, 1189-1202. https://doi.org/10.1126/science.192.4245.1189.

Fedorov, V. M., 2019, "Analysis of the Components of a Different Physical Nature in the Interannual Variability of the Total Solar Irradiance Flux", *Sol. Syst. Res.*, **53**, 376-382. https://doi.org/10.1134/S0038094619040026.

Forbush, S. E., 1954, "Worldwide cosmic-ray variations, 1937-1952", *J. Geophys. Res*., **59**, 525-542.

Haigh, J. D. Blackburn, M. and Day, R., 2005, "The response of tropospheric circulation to perturbations in lower-stratospheric temperature", *Journal of Climate*, **18**, 17, 3672-3685.

Hassan, D. Iqbal, A. Ahmad Hassan, S. Abbas, S. and Ansari, M. R. K., 2016, "Sunspots and ENSO relationship using Markov method", *Journal of Atmospheric and Solar-Terrestrial Physics*, **137**, 53-57. https://doi.org/10.1016/j.jastp.2015.11.017.

Hiremath, K. M., 2006, "The Influence of Solar Activity on the Rainfall over India : Cycle-to-Cycle Variations", *J. Astrophys. Astr.*, **27**, 367-372.

Hiremath, K. M. and Mandi, P. I., 2004, "Influence of the solar activity on the Indian Monsoon rainfall", *New Astron*., **9**, 651-662. https://doi.org/10.1016/j.newast.2004.04.001.

Gachari, F. Mulati, D. M. and Mutuku, J. N., 2014, "Sunspot numbers: Implications on Eastern African rainfall", *South African Journal of Science*, **110**, **1-2**, 69-74.

Gray, L. J. Beer, J. Geller, M. Haigh, J. D. Lockwood, M. Matthes, K. Cubasch, U. Fleitmann, D. Harrison, G. Hood, L. Luterbacher, J. Meehl, G. A. Shindell, D. Van Geel, B. and White, W., 2010, "Solar influences on climate", *Reviews of Geophysics*, **48**, 4, 1-53.

Jon Egill, K. and Jorn, Kristiansen, 2000, "Is there cosmic ray signal in recent variations n global cloudiness and cloud radiative forcing?", *J. Geophys. Res*., **105**, 11851-11863.

Kripalani, R. H. and Kumar, P., 2004, "Northeast monsoon rainfall variability over south peninsular India *vis-à-vis* the Indian Ocean dipole mode", *Int. J. Climatol*., **24**, 1267-1282. https://doi.org/10.1002/joc.1071.

Kumar, P. Rupa Kumar, K. Rajeevan, M. and Sahai, A. K., 2007, "On the recent strengthening of the relationship between ENSO and northeast monsoon rainfall over South Asia", *Clim. Dyn*.,**28**, 649-660. https://doi.org/10.1007/s00382-006-0210-0.

Lakshmi, S. Nivethaa, E.A.K. Ahamed Ibrahim, S. N. Ramachandran, A. and Palanivelu, K., 2021, "Prediction of Future Extremes During the Northeast Monsoon in the Coastal Districts of Tamil Nadu State in India Based on ENSO", *Pure Appl. Geophys*. https://doi.org/10.1007/s00024-021-02768-1.

Laurenz, L. Lüdecke, H.J. and Lüning, S., 2019, "Influence of solar activity changes on European rainfall", *Journal of Atmospheric and Solar-Terrestrial Physics*,**185**, 29-42.

Lean, L. J. J. Rottman, G. Kyle, H. L. N.Woods, T. R. Hickey, J. and C. Puga, L., 1997, "Detection and parameterization of variations in solar mid- and near-ultraviolet radiation (200-400 nm) Judith", *J. Geophys. Res*., **102**, 29939-29956.

Mendi, V., 2015, "El Nino: A Review", *Int. J. Earth Sci. Eng*., **8**, 130-137.

Nazari-Sharabian, M. and Karakouzian, M., 2020, "Relationship between Sunspot Numbers and Mean Annual Precipitation: Application of Cross-Wavelet Transform - A Case Study", *Journal of Multidiciplinary Scientific*, **3**, 1, 67-78.

Nitka, W. and Burnecki, K., 2019, "Impact of solar activity on precipitation in the United States", P*hysica A: Statistical Mechanics and its Applications*, **527**, 121387-96.

Pai, D.S. Sridhar, L. Rajeevan, M. Sreejith, O.P. Satbhai, N.S. and Mukhopadyay, B., 2014, "Development of a new high spatial resolution (0.25° × 0.25°) Long Period (1901-2010) daily gridded rainfall data set over India and its comparison with existing data sets over the region data sets of different spatial resolutions and time period", *MAUSAM*, **1**, 1-18.

Parker, E. N., 1999, "Sunny side of global warming", *Nature*, **399**, 416-417.

Poudel, P. Simkhada, S. and Adhikari, B., 2019, "Variation of Solar Wind Parameters Along With the Understanding of Energy Dynamics Within the Magnetospheric System During Geomagnetic Disturbances", *Adv. Earth Sp. Sci*., 276-293. https://doi.org/10.1029/2018EA000495.

Prestes, A., Rigozo, N. R., Echer, E. and Vieira, L. E. A., 2006, "Spectral analysis of sunspot number and geomagnetic indices (1868-2001)", *J. Atmos. Solar-Terrestrial Phys*., **68**, 182-190. https://doi.org/10.1016/j.jastp.2005.10.010.

Rajeevan, M. Unnikrishnan, C. K. Bhate, J. Niranjan Kumar, K. and Sreekala, P. P., 2012, "Northeast monsoon over India: Variability and prediction", *Meteorol. Appl*., **19**, 226-236. https://doi.org/10.1002/met.1322.

Rayner, N. A. Parker, D. E. Horton, E. B. Folland, C. K. Alexander, L. V. Rowell, D.P. Kent, E. C. and Kaplan, A., 2003, "Since the late nineteenth century, global analyses of sea surface temperature, sea ice, and night marine air temperature", *J. Geophys. Res. Atmos.*, **108**. https://doi.org/10.1029/ 2002jd002670.

Santos, J. L., 2006, "The impact of El Niño - Southern oscillation events on South America", *Adv. Geosci*., **6**, 221-225. https://doi.org/10.5194/adgeo-6-221-2006.

Sreekala, P. P. Rao, S. V. B. and Rajeevan, M., 2012, "Northeast monsoon rainfall variability over south peninsular India and its teleconnections", *Theor. Appl. Climatol*., **108**, 73-83. https://doi.org/10.1007/s00704-011-0513-x

Sreekala, P. P. Rao, S. V. B., Rajeevan, K. and Arunachalam, M. S., 2018, "Combined effect of MJO, ENSO and IOD on the intraseasonal variability of northeast monsoon rainfall over south peninsular India", *Climate Dynamics*, **51**, 9-10, 3865-3882.

Svensmark, H. Bondo, T. and Svensmark, J., 2009, "Cosmic ray decreases affect atmospheric aerosols and clouds", *Geophys. Res. Lett*., **36**, 1-4. https://doi.org/10.1029/2009GL038429.

Szypcio, Z. and Dolzyk-Szypcio, K., 2019, "Influence of Solar Activity on Total Annual Precipitation", *IOP Conference Series: Earth and Environmental Science*, **221**, 1.

Torrence, C. and Compo, G. P., 1998, "A Practical Guide to Wavelet Analysis", *Bull. Am. Meteorol. Soc*., **79**, 61-78.

Tsurutani, T. Goldstein, E. and Smith, J., 1990, "The interplanetary and solar causes of geomagnetic activity", *Planet. Sp. Sci*., **38**, 109-126.

Usoskin, I. G., 2005, "Solar activity , cosmic rays , and Earth ' s temperature : A millennium-scale comparison", *J. Geophys. Res*., **110**, 1-11. https://doi.org/10.1029/2004JA010946.

Usoskin, I. G. and Kovaltsov, G. A., 2008, "Cosmic rays and climate of the Earth: Possible connection", *Comptes Rendus - Geosci*., **340**, 441-450. https://doi.org/10.1016/j.crte.2007.11.001.

Vengateswari, M. Geethalakshmi, V. Bhuvaneswari, K. and Panneerselvam, S., 2019, "Influence of ENSO on wet and dry spell frequency for rainfed cropping period over Tamil Nadu", Int. Arch. Photogramm. Remote Sens. Spat. Inf. Sci. - ISPRS Arch". **42**, 63-65. https://doi.org/10.5194/isprs-archives-XLII-3-W6-63-2019.

Wang, B. Ding, Q. Fu, X. Kang, I. Jin, K. Shukla, J. and Doblas-Reyes, F., 2005, "Fundamental challenge in simulation and prediction of summer monsoon rainfall", *Geophysical Research Letters*, **32**, 15, 2-5.

Wang, R. Ma, H. Xiao, Z. Li, X. Gao, C. Gao, Y. Lai, A. and Li, X., 2021, "The Combined Effects of ENSO and Solar Activity on Mid-Winter Precipitation Anomalies Over Southern China", *Frontiers in Earth Science*, **9**, 1-15.

White, W. B. Cayan, D. R. and Lean, J., 1998, "Global upper ocean heat storage response to radiative forcing from changing solar irradiance and increasing greenhouse gas/aerosol concentrations", *Journal of Geophysical Research : Oceans*, **103**, C10, 21355-21366.

Yadav, R. K., 2012, "Why is ENSO influencing Indian northeast monsoon in the recent decades?", *Int. J. Climatol*., **32**, 2163-2180. https://doi.org/10.1002/joc.2430.

Zhai, Q., 2017, "Influence of solar activity on the precipitation in the North-central China", *New Astronomy*, **51**, 1339-1351.

Zhao, L., Wang, J., Zhao, H., 2012, "Solar Cycle Signature in Decadal Variability of Monsoon Precipitation in China", **90**, 1-9. https://doi.org/10.2151/jmsj.2012-101

Zubair, L. and Ropelewski, C. F., 2006, "The strengthening relationship between ENSO and northeast monsoon rainfall over Sri Lanka and southern India", *J. Clim*., **19**, 1567-1575. https://doi.org/10.1175/JCLI3670.1**.**